MID-AMERICA TRANSPORTATION CENTER

Report # MATC-MS&T: 128-2

Final Report
WBS: 25-1121-0005-128-2

Development of ATMA Deployment Guidelines Considering Traffic and Safety Impacts

Xianbiao Hu, PhD
Assistant Professor
Department of Civil and Environmental Engineering
Pennsylvania State University

Qing Tang
PhD Student
Department of Civil and Environmental Engineering
Pennsylvania State University

Genda Chen, PhD, PE, F.ASCE
Professor and Abbett Distinguished Chair
Department of Civil, Architectural and Environmental Engineering
Missouri University of Science & Technology

2022

A Cooperative Research Project sponsored by
U.S. Department of Transportation- Office of the Assistant Secretary for Research and Technology

Development of ATMA Deployment Guidelines Considering Traffic and Safety Impacts

Xianbiao Hu, Ph.D.
Assistant Professor
Department of Civil and Environmental Engineering
Pennsylvania State University

Qing Tang, Ph.D. Student
Department of Civil and Environmental Engineering
Pennsylvania State University

Genda Chen, Ph.D., P.E., F. ASCE
Professor and Abbett Distinguished Chair
Department of Civil, Architectural and Environmental Engineering
Missouri University of Science and Technology

A Report on Research Sponsored by

Mid-America Transportation Center
University of Nebraska–Lincoln

October 15, 2022

Technical Report Documentation Page

1. Report No. 25-1121-0005-128-2	2. Government Accession No.	3. Recipient's Catalog No.
4. Title and Subtitle Development of ATMA Deployment Guidelines Considering Traffic and Safety Impacts		5. Report Date October 12, 2022 6. Performing Organization Code
7. Author(s) Xianbiao Hu, PhD, ORCID: https://orcid.org/0000-0002-0149-1847 Qing Tang; Genda Chen;		8. Performing Organization Report No. 25-1121-0005-128-2
9. Performing Organization Name and Address Mid-America Transportation Center 2200 Vine St. PO Box 830851 Lincoln, NE 68583-0851		10. Work Unit No. 11. Contract or Grant No. 69A3551747107
12. Sponsoring Agency Name and Address Missouri University of Science and Technology 1201 N State St., Rolla, MO 65409 Pennsylvania State University 212 Sackett Building. University Park, PA 16802.		13. Type of Report and Period Covered Final Report (1/2020-12/2022) 14. Sponsoring Agency Code MATC TRB RiP No. 91994-57
15. Supplementary Notes		

16. Abstract

The Autonomous Truck Mounted Attenuator (ATMA) vehicle system is a quickly emerging technology that leverages connected and autonomous vehicle (CAV) capabilities for maintenance of transportation infrastructure. Because practicable and implementable guidance for deployment of this technology is largely missing in MUTCD, State DOTs have been making their own deployment criteria. In this project, we focus on the Operational Design Domain (ODD) problem, i.e., under what traffic conditions should ATMA be deployed. To this end, modeling efforts are first focused on the derivation of an effective discharge rate that can be associated with a moving bottleneck that is caused by slow-moving ATMA vehicles on a multilane highway. Then, based on the demand input and discharge rates, microscopic traffic flow models are employed to calculate vehicle delay and traffic flow density, which the Highway Capacity Manual (HCM) suggests are key indicators of a multilane highway's level of service (LOS). In this way, the linkage between AADT and LOS is analytically established. NGSIM data is used for the model validation and shows that the developed model correctly captures the effective discharge rate discount caused by moving bottlenecks. The modeling results demonstrate that roadway performance is sensitive to the K factor and D factor, as well as the operating speed of ATMA and, if LOS=C is a desirable design objective, a good AADT threshold to use would be around 40,000 vehicles per day.

17. Key Words Autonomous Truck Mounted Attenuator (ATMA); Operational Design Domain (ODD); Effective Discharge Rate; Moving Bottleneck; Level of Service (LOS);	18. Distribution Statement No restrictions.		
19. Security Classif. (of this report) Unclassified	20. Security Classif. (of this page) Unclassified	21. No. of Pages 38	22. Price

Form DOT F 1700.7 (8-72) Reproduction of completed page authorized

Table of Contents

List of Abbreviations v
Disclaimer vi
Abstract vii
Chapter 1 Introduction 1
Chapter 2 Preliminaries 6
2.1 ATMA Introduction 7
2.2 Performance Measurement of Multilane Highways 9
2.3 Discharge Rate Under Normal Traffic Conditions 10
2.4 Queue Length and Delay 12
Chapter 3 Analytical Derivation of Performance Measures 15
3.1 Problem Setup 15
3.2 Derivation of Discounted Capacity with Moving Bottleneck 16
3.3 LOS Derivation 21
Chapter 4 Numerical Analysis 24
4.1 Effective Discharge Rate Validation 24
4.2 Typical Scenario ODD Analysis 28
4.3 Sensitivity Analysis 30
4.3.1 When K-factor changes 32
4.3.2 When operating speeds of the ATMA vehicles change 33
Chapter 5 Conclusions 35
References 37

List of Figures

Figure 2.1 ATMA Vehicle System: (a) system overview; (b) view from above; and (c) view from the rear. 8
Figure 2.2 LOS on Base Speed-Flow curves from HCM (2010). 10
Figure 2.3 (a) Time-space diagram of Newell's car-following model and (b) triangular fundamental diagram. 11
Figure 2.4 Queue formation and dissipation processes. 14
Figure 3.1 Schematic diagram of a four-lane highway (one direction) segment with ATMA vehicles. 16
Figure 3.2 Flow-density relationship from both a moving observer's view and a stationary observer's view. 18
Figure 4.1 An illustration of the study area: Northbound I-80. 24
Figure 4.2 Vehicle trajectory for lanes 5 and 6, I-80, NGSIM. 25
Figure 4.3 Vehicle trajectory of trucks (IDs:2862 and 1522), I-80, NGSIM. 27
Figure 4.4 APE comparison of six slower trucks, I-80, NGSIM. 28
Figure 4.5 Relationship between AADT, average vehicle delay and traffic density. 29
Figure 4.6 Proposed relationship between AADT and (a) average delay and (b) LOS when D changes. 32
Figure 4.7 Proposed relationship between the AADT and (a) average delay and (b) LOS when K changes. 33
Figure 4.8 Proposed relationship between the AADT and (a) average delay and (b) LOS when the operating speed of an ATMA changes. 34

List of Abbreviations

Autonomous Maintenance Technology (AMT)
Autonomous Truck Mounted Attenuator (ATMA)
Automated Driving System (ADS)
Connected and Autonomous Vehicle (CAV)
Cross Track Error (CTE)
Department of Transportation (DOT)
Follower Truck (FT)
Global Positioning System (GPS)
Lead Truck (LT)
Missouri Department of Transportation (MoDOT)
Operator Control Unit (OSU)
Radio Frequency (RF)
Sensitivity Analysis Factor (SAF)
System Control Unit (SCU)
User Interface (UI)
Vehicle-to-Vehicle (V2V)

Disclaimer

The contents of this report reflect the views of the authors, who are responsible for the facts and the accuracy of the information presented herein. This document is disseminated in the interest of information exchange. The report is funded, partially or entirely, by a grant from the U.S. Department of Transportation's University Transportation Centers Program. However, the U.S. Government assumes no liability for the contents or use thereof.

Abstract

The Autonomous Truck Mounted Attenuator (ATMA) vehicle system is a quickly emerging technology that leverages connected and autonomous vehicle (CAV) capabilities for maintenance of transportation infrastructure. Promoted by FHWA and about a dozen State DOTs, it is a niche CAV application in leader-follower style that removes DOT workers from the following maintenance truck, in order to reduce fatalities in work zone locations. Because practical and implementable guidance for deployment of this technology is largely missing in MUTCD, State DOTs have been making their own deployment criteria. For example, Colorado DOT is using annual average daily traffic (AADT) of less than 6,000 as the criteria to identify low-volume roads for ATMA deployment. In this project, we focus on the Operational Design Domain (ODD) problem, i.e., under what traffic conditions should ATMA be deployed. To this end, modeling efforts are first focused on the derivation of an effective discharge rate that can be associated with a moving bottleneck that is caused by slow-moving ATMA vehicles on a multilane highway. Then, based on the demand input and discharge rates, microscopic traffic flow models are employed to calculate vehicle delay and traffic flow density, which the Highway Capacity Manual (HCM) suggests are key indicators of a multilane highway's level of service (LOS). In this way, the linkage between AADT and LOS is analytically established. NGSIM data is used for the model validation and shows that the developed model correctly captures the effective discharge rate discount caused by moving bottlenecks. The modeling results demonstrate that roadway performance is sensitive to the K factor and D factor, as well as the operating speed of ATMA and, if LOS=C is a desirable design objective, a good AADT threshold to use would be around 40,000 vehicles per day.

Keywords: Autonomous Truck Mounted Attenuator (ATMA); Operational Design Domain (ODD); Effective Discharge Rate; Moving Bottleneck; Level of Service (LOS);

Chapter 1 Introduction

America's roads are critical for moving an ever-increasing number of people and goods. Unfortunately, the growing wear and tear to our nation's roads have left 43% of our public roadways in poor or mediocre condition [1]. In 2020 alone, USDOT spent a total of $24 Billion dollars to preserve national highway systems. Mobile and slow-moving operations, such as striping, sweeping, bridge flushing, and pothole patching, are critical for the efficient and safe operation of a highway transportation system. Performing the maintenance required for a roadway infrastructure, however, could involve risks, and many work zone crashes involved State Department of Transportation (DOT) workers. For example, in the State of Missouri, slow-moving operation vehicles have been involved in crashes more than 80 times since 2013, resulting in many injuries to DOT workers [2]. Reducing hazards and achieving a safer environment for DOT workers remains an urgent problem.

The Autonomous Truck Mounted Attenuator (ATMA) vehicle system is a quickly emerging technology that combines the use of connected and autonomous vehicle (CAV) capabilities and Autonomous Maintenance Technology (AMT), to maintain the transportation infrastructure in work zones. Promoted by FHWA and many State DOTs, ATMA is a niche CAV application in leader-follower style that removes DOT workers from the following maintenance truck to reduce fatalities in work zones. For example, Colorado and Missouri are among the first States in the U.S. to test and deploy ATMA vehicles to remove DOT workers from the driver seat [3, 4]. Several other States, including California, Minnesota, Virginia, Ohio, North Dakota, and Tennessee [5] are in the process of testing, or deploying similar technologies. In addition, Colorado DOT is leading an autonomous maintenance technology pool fund with 13

State DOT members [6], together with the FHWA. A brief introduction of the ATMA system is presented in Section 2 and can also be found in [4].

Despite the fact the ATMA technology is being rapidly developed and deployed, the practical and implementable guidance for its deployment is largely missing in the Manual on Uniform Traffic Control Devices (MUTCD) and other federal regulations and national standards. Without such guidance, State DOTs have been making their own criteria to answer the question of when and where to deploy ATMA. For example, Colorado DOT is using an annual average daily traffic (AADT) of less than 6,000 as the criteria to identify low-volume roads for ATMA deployment. This is because, due to the nature of mobile and slow-moving operations, ATMA vehicles are usually driving slowly (such as 5~15mph) and, as such, the argument is to avoid slowing traffic on a busy corridor during peak hours. A problem with this criterion is that AADT on multilane highways varies for different DOTs. Roads with an AADT lower than 6,000 might be common in Colorado, but in other States, such as California and New York, most roads are much busier than that. So, the question is whether this AADT threshold is reasonable, and how we should develop a sound method to scientifically determine this threshold.

To bridge this important gap, this project aims to develop microscopic traffic flow models to identify the Operational Design Domain (ODD) of ATMA, on a typical multilane highway. Learning from the Highway Capacity Manual (HCM) [7], six measures can be used to determine the level of service (LOS) of a multilane highway, namely speed, delay, throughput, density, environmental, and the ratio of demand/capacity. As such, in this research, we choose total delay, as well as traffic density, as the performance measurements, to quantitatively evaluate the impact of ATMA vehicles on traffic flow, and to support the identification of ODD. However, the key challenge in quantifying delay and traffic density is the calibration of capacity

drop caused by the ATMA system. This is due to the slow operating speed of the ATMA system, compared with the other fast-moving traffic, so that it, essentially, becomes a moving bottleneck and discounts traffic flow capacity. As such, an accurate modeling of a moving bottleneck capacity drop becomes a prerequisite for the quantification of traffic flow performance.

Some modeling efforts to derive an effective roadway discharge rate that is affected by a moving bottleneck can be found in the literature. For example, Leclercq et al. [8] proposed an analytical model that extended the Newell-Daganzo model by endogenously incorporating a capacity drop related to the merging process. This work was extended by Leclercq et al. [9] by accounting for heterogeneous vehicle characteristics and the physical interactions between upstream waves and downstream voids, and by estimating the effective capacity for a freeway merger in a multilane context [10]. However, an explicit analytical expression of capacity drop was not available in these works, and a system of four equations and four unknowns was listed for computing the numerical solutions. Yuan et al. [11] investigated to determine to what extent the acceleration spread and reaction time could influence the queue discharge rate, as well as proposing a speed dependent reaction time mechanism to give variable queue discharge rates. Laval and Daganzo [12] focused on freeway sections, away from diverges, where the main incentive for drivers to change lanes was by increasing their speed. Mathematical models were developed to describe the mechanism of lane-changing vehicles, that created voids in traffic streams, and how these voids reduced flow. Chen and Ahn [13] investigated how spatially distributed lane changes impacted capacity-drop at an extended merge, diverge, and weave bottlenecks, and developed analytical models to capture the impacts of lane changes and numerical simulations to quantify capacity drop. Other freeway capacity-drop modeling efforts can be referred to in [14-18], among others. However, these models are usually complicated and

lack an explicit analytical expression, which greatly limits their applications in real-world problems. This is particularly the case for the problem that we are studying, as the ATMA system is not a common moving bottleneck. The system includes a minimum of two vehicles, including one manned leader truck, and at least one unmanned follower truck, and there is a gap distance of 100~1,000 ft between these two vehicles. As such, the previous moving bottleneck models become not applicable.

As such, in this project, modeling efforts are first focused on the analytical derivation of an effective discharge rate that is associated with the moving bottleneck caused by ATMA vehicles. Such analytical derivation is based on the fundamental diagram with moving coordinates. The derived effective discharge rates are represented with mathematically-simple expressions in a closed-form, and correctly account for the effects of demand inputs (i.e., arrival rate on the highway), real time traffic status (e.g., cruising speed of general traffic, and the operation speed of ATMA), as well as the traffic flow characteristics (such as backward wave speed and jam density). Next, microscopic traffic flow models are employed, so that once the discounted capacity is obtained, it can be combined with the highway traffic's arrival rate, to calculate the vehicle delay and traffic flow density, which are chosen as the key indicators of a multilane highway level of service. In this way, the linkage between demand (e.g., AADT) and LOS are analytically established and, based on such relationships, numeric analysis is performed to quantitively determine the ODD of ATMA.

This report is organized as follows. Chapter 2 includes an ATMA system overview, performance measures of multilane highways, and the discharge rate and queuing profile of traffic flow. Chapter 3 focuses on the development of methodology in which the analytical derivations of the effective discharge rate and total delay for a four-lane highway segment are

presented. In Chapter 4, the developed model is validated with a NGSIM dataset, and the modeling result analysis and sensitivity analysis are discussed. Chapter 5 concludes this report.

Chapter 2 Preliminaries

In this chapter, we will briefly introduce the ATMA system, followed by a review of performance measurement on multilane highways from HCM. Then, we show how to derive the effective discharge rate, based on a triangle fundamental diagram, a process to calculate the length of the queue, and the delay of traffic flow.

The notations used in this report include:

Notation	Definition
t	timestamp
$n, n-1$	indexes of following and leading vehicle, respectively
τ_n, d_n	response time and temporal delay of vehicle n
v_1, v_2	speeds before and after the speed changes
$h_{n,1}, h_{n,2}$	time headway of vehicle n before and after the speed changes
$s_{n,1}, s_{n,2}$	space headway of vehicle n before and after the speed changes
q, k, v	traffic flow, density and speed
$\bar{\tau}, \bar{d}$	arithmetic average of the τ and d
v_f, k_j	free-flow speed and jam density
v_u	cruising speed on the four-lane highway segment. Due to bottleneck or congestion, $v_u \leq v_f$
w	backward wave speed
μ	maximum discharge rate
$\lambda(t)$	time-dependent arrival rate
t_0, t_1	time that queue starts, and time to reach the maximum arrival rate
$t_2, \bar{t}$	time with longest queue, and time when the queue is fully discharged
$Q(t)$	time-dependent queue length

Notation	Definition
W	total delay
N	total number of vehicles that enter a roadway segment
v_{lt}	speed of the ATMA vehicles
θ	discount factor of the effective discharge rate
$x^*(t)$	location of a moving observer relative to the entering vehicle
$q^*(t)$	flow rate at which vehicle pass the observer who is travelling at a speed of $v^*(t)$
$Q(k), Q^*(k)$	flow as a function of density seen from stationary and moving coordinates
$\lambda_{\mathrm{in}}(t), \lambda'_{\mathrm{in}}(t)$	adjusted flow rate from stationary coordinate and moving coordinate
APE	absolute percentage error
$\bar{W}$	average delay during the AMTA vehicles performing maintenance
$\bar{t}$	average travel time on the four-lane highway segment
$\tilde{k}$	estimated density on the four-lane highway

2.1 ATMA Introduction

The Autonomous Truck Mounted Attenuator vehicle, sometimes referred to as Autonomous Impact Protection Vehicle (AIPV), is a quickly emerging technology and offers a promising solution to eliminate injuries to DOT workers while performing roadway maintenance. Figure 2.1 below shows some pictures of an ATMA vehicle system under operation on a roadway, which shows (a) an overview of the system, (b) a view from above, and (c) a view from the rear. The vehicle system consists of a manned leader truck, an unmanned follower truck, and a truck mounted attenuator (TMA) installed on the follower truck. The leader truck is designed to perform the regular maintenance work, whereas the follower truck is

designed to drive autonomously and duplicate the behavior of the leader truck, as well as to serve as a buffer in case a crash happens. The distance between the leader truck and the follower truck is usually small, e.g., 100~200 ft. As a result, the leader-follower design significantly simplifies the self-driving scenario and allows the follower truck to simply mimic the action of the leader truck. The idea is that, in case a highway crash is inevitable at a work zone location, the follower vehicle will be hit first and, since it does not have a human driver and is equipped with TMA, the DOT workers' lives will be saved. Actuators, software, electronics, and vehicle-to-vehicle (V2V) communication equipment are installed on the leader truck and the follower truck and, together, they enable connectivity (mainly V2V) and the autonomous driving capabilities of a leader-follower style.

(a)

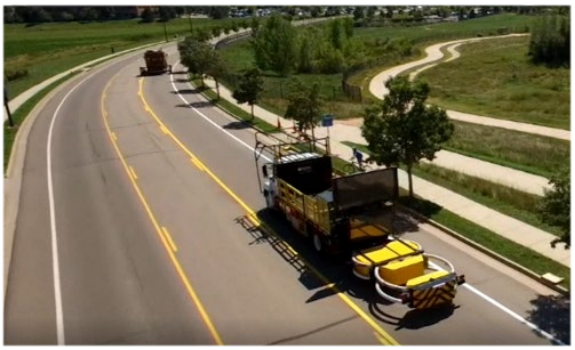

(b)

(c)

Figure 2.1 ATMA Vehicle System: (a) system overview; (b) view from above; and (c) view from the rear.

2.2 Performance Measurement of Multilane Highways

LOS is a quantitative stratification of a performance measure that represents quality of service. Serval measures are mainly defined by HCM [7] to evaluate the LOS of multilane highways: 1) Density, which is typically defined by the average number of vehicles per lane per mile of roadway; 2) Speed, which reflects how fast motorists can travel along a roadway. Drivers experience delays when their travel speed is less than free-flow speed, which is a result of traffic demands that approach or exceed the roadway's capacity; 3) Volume-to-capacity (v/c) ratio, which reflects how closely a roadway is operating at capacity, as well as 4) vehicle delay, 5) traffic throughput, and 6) environmental conditions.

Figure 2.2 describes how speed and density determine LOS under different free-flow speeds (FFS) for multilane highways [7]. In other words, on a standard multilane highway, and under normal conditions, if the designed FFS is given, this plot can be used to very easily determine the LOS of any traffic flow. However, as discussed above, in the event of highway maintenance, the moving bottleneck, generated by ATMA vehicles, leads to capacity reduction, which fundamentally changes the volume-speed relationship in this diagram. As such, an accurate modeling of a moving bottleneck capacity drop becomes a prerequisite and, once the capacity of the moving bottleneck is obtained, we can employ microscopic traffic flow models to calculate the resulting vehicle delay and traffic flow density. Then, these measurements can be compared with the thresholds in Figure 2.2 to determine the LOS of the highway segment.

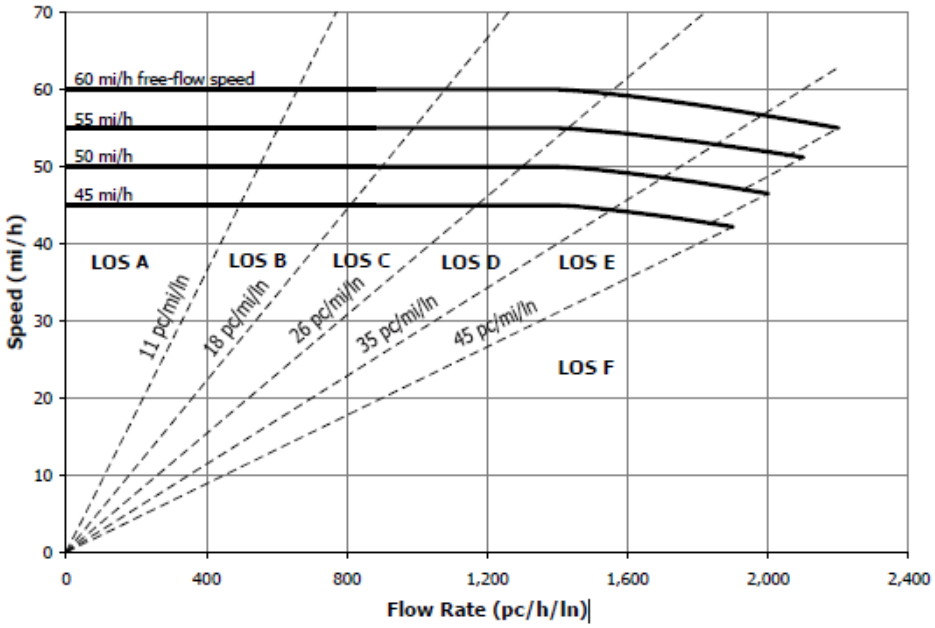

Figure 2.2 LOS on Base Speed-Flow curves from HCM (2010).

2.3 Discharge Rate Under Normal Traffic Conditions

In this section, we review how to derive the discharge rate (i.e., highway capacity) under normal traffic conditions. A simplified car-following model was proposed by Newell [19] and adopted in this report to describe a vehicle's kinematic movements on a roadway segment. The simplified model states that the time-space trajectory of a following vehicle n is essentially the same as its leading vehicle $n-1$, except for a delay in space and time. In the time-space diagram (shown in Figure 2.3-a below), a leading vehicle $n-1$ initially drives at a constant speed v_1 and then changes to another constant speed v_2. According to the simplified car-following model, the following vehicle n also travels at the same speed of v_1 at the beginning, and then changes to the v_2 speed. However, at the turning point, there is a temporal delay of τ_n which represents the driver n's necessary response time, as well as a spatial delay of d_n, which represents the distance needed to ensure safe driving.

Following vehicle n's movement trajectory can be calculated by $x_n(t+\tau_n) = x_{n-1}(t) + d_n$. Based on the time-space diagram, the time headway of n's vehicle before and after speed change can be derived with $h_{n,1} = \tau_n + \frac{d_n}{v_1}$ and $h_{n,2} = \tau_n + \frac{d_n}{v_2}$, respectively. The space headway of n's vehicle before and after the speed changes can be computed by $s_{n,1} = d_n + \tau_n \cdot v_1$ and $s_{n,2} = d_n + \tau_n \cdot v_2$, respectively.

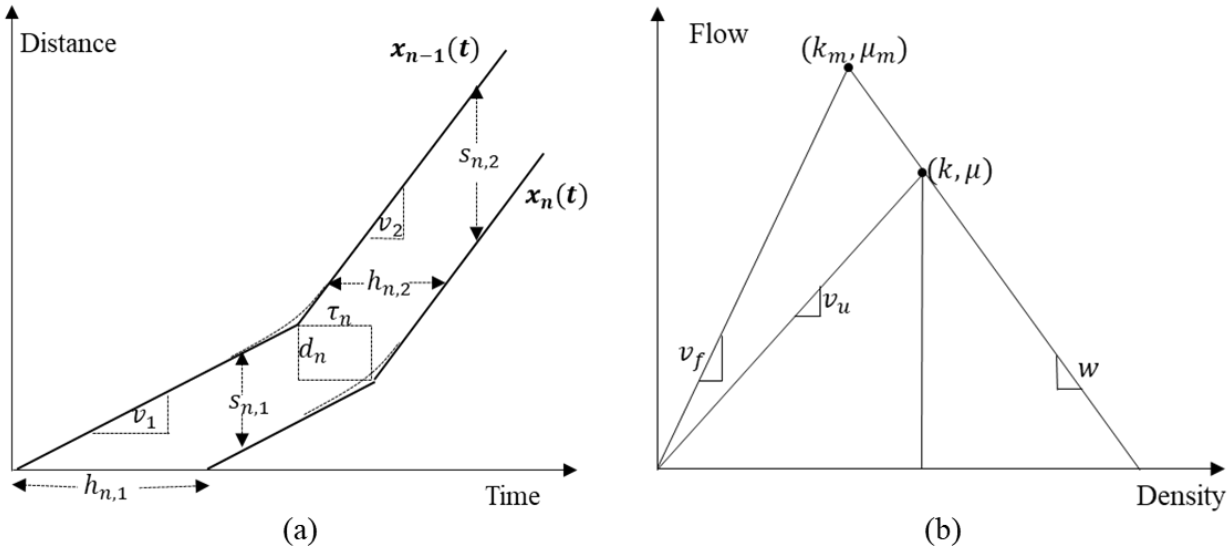

Figure 2.3 (a) Time-space diagram of Newell's car-following model and (b) triangular fundamental diagram.

The Newell car-following model above suggests the triangular fundamental diagram that is shown in Figure 2.3-b. Per [19], the q-k relationship can be represented as $q = \frac{1}{\bar{\tau}} - \frac{\bar{d}}{\bar{\tau}}k$, in which $\bar{\tau} = \frac{1}{n}\sum_{k=1}^{n}\tau_k$ and $\bar{d} = \frac{1}{n}\sum_{k=1}^{n} d_k$. The fundamental diagram has a free flow speed v_f, backward wave speed w, maximum discharge rate μ_m and its corresponding density k_m, and jam density k_j. Of the five variables, if three of them are known, the remaining two can be derived.

Following the above-mentioned fundamental diagram, when v_f, w, and k_j are known for a roadway segment, its maximum discharge rate μ_m can be calculated as $\mu_m = \frac{k_j}{(\frac{1}{v_f}+\frac{1}{w})} = \frac{k_j \cdot v_f \cdot w}{v_f + w}$.

It should be noted that μ_m is the maximum discharge rate under prevailing traffic conditions. In the case of congestion (e.g., due to lane drop or other geometric reasons), the actual cruising speed may be lower than the free-flow speed. We used a new point (k, μ) in the q-k diagram in Figure 2.3-b to represent the discharge rate due to the congestion impact, with $\mu < \mu_m$. The cruising speed is denoted as v_u, with $v_u < v_f$, the new discharge rate becomes Equation (2.1) in a generic form.

$$\mu = \frac{k_j}{(\frac{1}{v_u}+\frac{1}{w})} = \frac{k_j \cdot v_u \cdot w}{v_u + w} \tag{2.1}$$

2.4 Queue Length and Delay

Based on the classical work by Newell in using a fluid-based approximation method to characterize the queue formation and dissipation processes [20], we consider two types of states: uncongested and congested. Under the congested state with homogeneous traffic, we consider a single value of μ.

We denote the time-dependent arrival rate (i.e., the demand) as $\lambda(t)$. During off-peak hours, $\lambda(t) < \mu$ and no queue exists (to be exact, when a moving bottleneck is present, the discounted capacity μ' should be used, but for the sake of simplicity, we still use μ here). When the demand increases and finally exceeds the μ, vehicles start to form a queue. The queue dissipates and traffic returns to normal, as demand reduces after peak hours. Figure 2.4 provides

an illustration of the demand-supply relationship and queuing profile. In Figure 2.4(a), the demand (black curve OABCE) exceeds the maximum discharge rate (red horizontal line AD) during the peak hour between t_0 and t_2, and the queue formation is illustrated by the area highlighted by red lines (i.e., ABCA). The arrival rate reaches peak at time t_1. The longest queue is observed at time t_2 and starts to shrink, as shown by the green lines (i.e., area CDEC). The queue is fully discharged at time $\bar{t}$. The queuing profile is illustrated in Figure 2.4(b).

Based on the illustration in Figure 2.4, the length of the queue at time t can be derived by $Q(t) = \int_{t_0}^{t} (\lambda(\tau) - \mu) d\tau$. The total delay is, thus, the integral of queue length from t_0 to t_3, which can be calculated by Equation (2.2).

$$W = \int_{t_0}^{t_3} Q(t) d\tau = \int_{t_0}^{\bar{t}} Q(t) d\tau \tag{2.2}$$

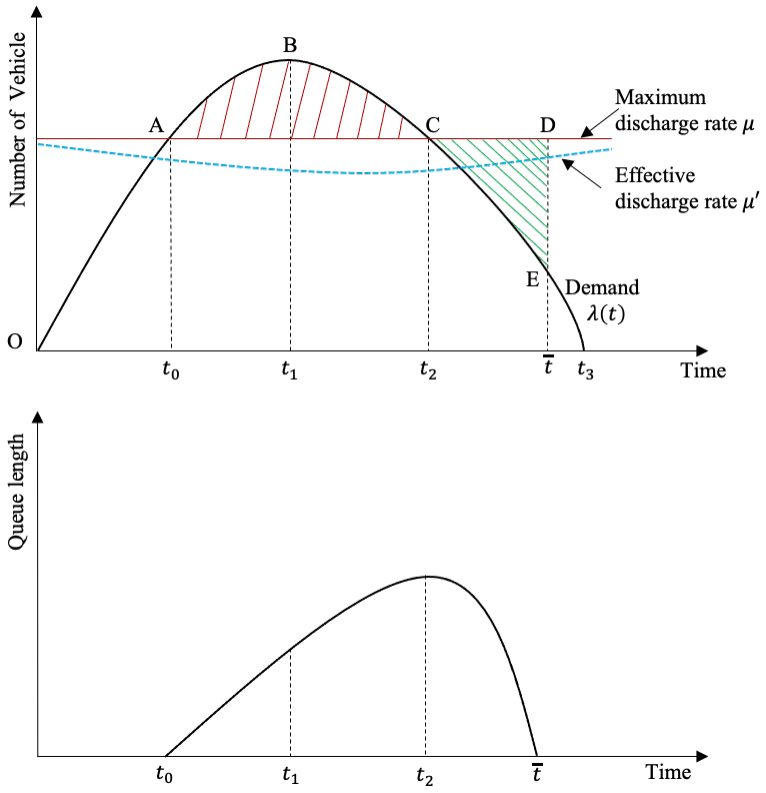

Figure 2.4 Queue formation and dissipation processes.

Chapter 3 Analytical Derivation of Performance Measures

3.1 Problem Setup

In this section, we focus on a typical highway with two lanes of the same direction, and the traffic on both lanes going to the right side, as shown in Figure 3.1. The ATMA vehicle system is represented by the two vehicles in the red box, with a leader truck (LT) and a follower truck (FT), and a gap distance of L_{gap} between these two vehicles. The other general vehicles are represented by a smaller black vehicle icon.

The total in-flow rate is $\lambda(t)$ for both lanes. The lane flow distribution is presented by α, so the left lane has a flow rate of $\alpha * \lambda(t)$, whereas the right-lane has a flow rate of $(1-\alpha) * \lambda(t)$. The cruising speed of general traffic is v_{u}, and ATMA vehicles drive at a constant speed of v_{lt} (where lt stands for leader truck). v_{lt} is usually between 5~15mph and is, thus, much slower than v_{u}, i.e., $v_{\text{lt}} < v_{\text{u}}$ and, as such, the ATMA can be considered as a moving bottleneck in the two-lane highway segment. As a result, the vehicles behind the ATMA vehicles (represented by red colored small cars in Figure 3.1) can switch to the left lane to bypass the moving bottleneck. Note that, although for simplicity a two-lane highway is used, the proposed model can be iteratively applied to a highway with three or more lanes.

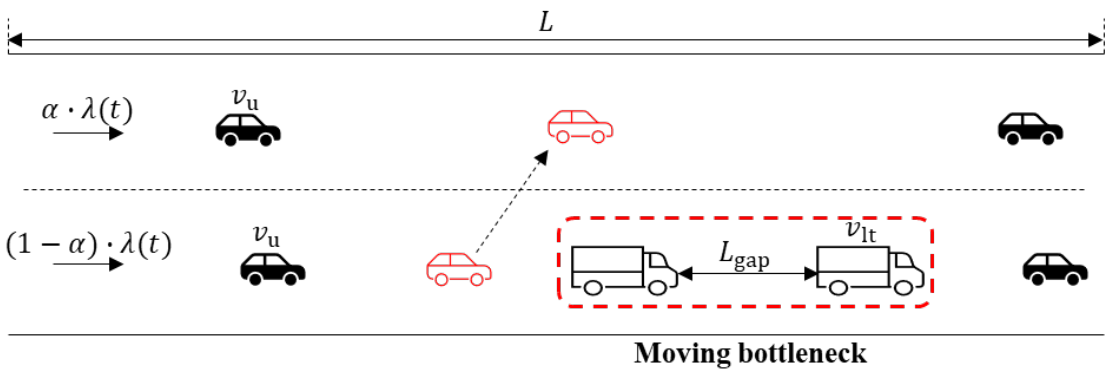

Figure 3.1 Schematic diagram of a four-lane highway (one direction) segment with ATMA vehicles.

3.2 Derivation of Discounted Capacity with Moving Bottleneck

Next, we will analytically derive the discounted capacity (or, effective discharge rate), influenced by this moving bottleneck. We follow the theory from Newell [21], that a moving coordinate system, traveling at speed v_{lt}, can be transformed into a corresponding analysis of flow past a stationary bottleneck, with some proper coordinate transformation.

We start by placing a "moving observer" on the main road who is traveling at the same velocity v_{lt} as the ATMA vehicles, at any time t, at a location $x^*(t)$ relative to the ATMA vehicles. The equation from Newell [21], on the derivation of $x^*(t)$, is given in Equation (3.1). In our problem, since they travel at the same speed, $x^*(t)$ remains a constant. Next, we also place a "stationary observer" on the main road, whose location does not change.

$$x^*(t) = x(t) - v_{lt} \cdot t \tag{3.1}$$

As the moving observer moves at the same speed as the ATMA vehicles, from his perspective, the two-lane roadway segment becomes a stationary section of road with only one

lane for the other vehicles adjacent to ATMA vehicles. From his perspective, there is a lane reduction with a capacity drop. Some vehicles merge from two lanes to one lane, pass this bottleneck location, and then switch lanes to drive again on a two-lane roadway segment (again, please refer to the red vehicles in Figure 3.1). Let us call the view from the moving observer's perspective "moving coordinates", and the view from the stationary observer's perspective "stationary coordinates". Based on such definitions, the target of this section, i.e., the moving bottleneck capacity, is the maximum discharge rate from a stationary observer's perspective, with the presence of ATMA vehicles. The below equation shows how to derive such a value step by step.

Assume that the flow and the density of the one lane and two lanes have a functional relationship in the stationary coordinates, i.e. $q = Q_1(k)$ and $q = Q_2(k)$. If we use $q^*(t)$ to denote the rate at which vehicles on the main road pass the moving observer, who is travelling at a speed of v_{lt}, then

$$q^*(t) = q - k \cdot v_{\mathrm{lt}} \tag{3.2}$$

The density of the one-lane and the two-lane roadway segments are the same, no matter whose perspective (moving observer or stationary observer) is adopted. The relationship between $q^*(t)$ and k can be derived as:

$$q^*(t) = Q_1(k) - k \cdot v_{\mathrm{lt}} = {Q_1}^*(k), \qquad q^*(t) = Q_2(k) - k \cdot v_{\mathrm{lt}} = {Q_2}^*(k) \tag{3.3}$$

In which $Q_1{}^*(k)$ and $Q_2{}^*(k)$ represent the q-k relationship of a one-lane and a two-lane roadway segment, as seen from the moving observer's perspective.

Figure 3.2 presents q-k fundamental diagrams of a one-lane and a two-lane roadway from both a moving observer's and a stationary observer's perspectives. The moving observer's view is marked with red (i.e., OGI), and the stationary observer's view is marked with black (i.e., $OG'I'$). The moving bottleneck's speed is fixed at v_{lt}. Note the triangle O-F-L is the fundamental diagram of the one-lane segment, and triangle O-G-I is the fundamental diagram of the two-lane segment in the moving coordinate. As discussed by Newell [21], if a flow of $k \cdot v_{\mathrm{lt}}$ is added to q^*, the resulting FD will be in the stationary coordinates. As such, the triangle O-F'-L' is the fundamental diagram of the one-lane segment and triangle O-G'-I' is the fundamental diagram of the two-lane segment in the stationary coordinates. The angle of $\angle G'OI' = arctan\, v_{\mathrm{u}}$, angle of $\angle I'OI = arctan\, v_{\mathrm{lt}}$, and the angle of $\angle G'I'O = arctan\, w$.

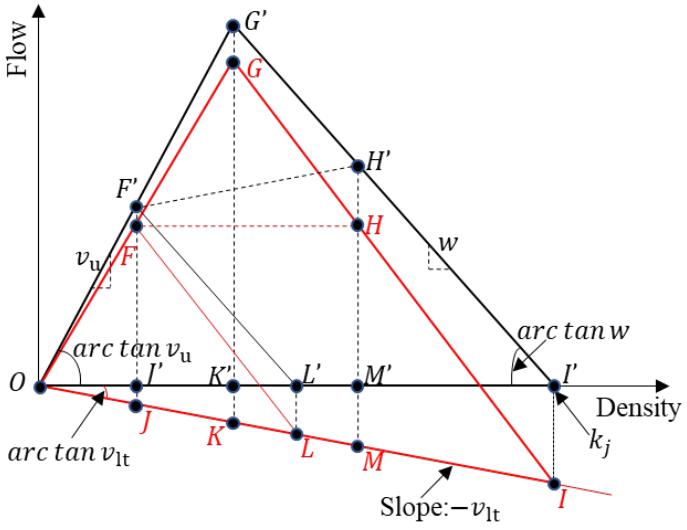

Figure 3.2 Flow-density relationship from both a moving observer's view and a stationary observer's view.

We first calculate the adjusted flow rate $\lambda_{in}{}'(t)$ in the moving coordinate system. At any given time t, there is an incoming flow rate $\lambda_{in}(t)$ and the moving bottleneck's speed v_{lt}. To convert that into the adjusted flow rate $\lambda_{in}{}'(t)$ in the moving coordinate system, the density is calculated on the two-lane roadway segment with $Q_2(\, k_2) = \lambda_{in}(t)$, or $k_2 = Q_2{}^{-1}\big(\lambda_{in}(t)\big)$. Then, the adjusted flow rate $\lambda_{in}{}'(t)$ can be calculated as

$$\lambda_{in}{}'(t) = \lambda_{in}(t) - k_2 \cdot v_{\mathrm{lt}} = \lambda_{in}(t) - Q_2{}^{-1}\big(\lambda_{in}(t)\big) \cdot v_{\mathrm{lt}} \tag{3.4}$$

For example, in the stationary coordinate system, $F'J'$ is the maximum discharge rate of the one-lane segment, in which $F'J'$ is perpendicular to OI' and OJ' is its corresponding density. Following this with Equation (3.4), to calculate the maximum discharge rate of the one-lane segment in the moving coordinate system, $F'J'$ must be reduced by $OJ' \cdot v_{\mathrm{lt}}$ which is JJ' and, thus, becomes FJ'. In other words, FJ' is the maximum discharge rate of the one-lane segment in the moving coordinate system.

In the moving coordinate system, if $\lambda_{in}{}'(t) < FJ'$, all vehicles can pass through the moving bottleneck at full cruising speed v_{u}. Otherwise, the adjusted arrival rate $\lambda_{in}{}'(t)$ becomes higher than the maximum discharge rate and, thus, the ATMA vehicles become a moving bottleneck, and the roadway segment is subject to a maximum discharge rate with a value of FJ'. Subsequently, the traffic state of the downstream bottleneck location is represented by point F, while that of the bottleneck upstream is represented by point H, which has the same outflow rate as point F (i.e., $y_F = y_H$,) but with a higher density due to the queue. F and H become points F' and H' when the moving coordinates are converted back to the stationary coordinates points after adding a flow of $k \cdot v_{\mathrm{lt}}$, i.e. $y_{F'} = y_F + k_F v_{\mathrm{lt}}$ and $y_{H'} = y_H + k_H v_{\mathrm{lt}}$. Since the density at point

H is higher than that at point F (i.e., $k_H > k_F$), the flow rate at point H' is also higher than that at point F' (i.e., $y_{H'} > y_{F'}$), Thus, it is point H' that determines the maximum discharge rate instead of point F' in the stationary coordinate system.

Next, we derive the length of $H'M'$, which is the maximum discharge rate of point H' in the stationary coordinate system (i.e., our target capacity with a moving bottleneck). First, let us look at the triangle of F-O-L, which is the fundamental diagram of a one-lane roadway. As $F'J'$ is the maximum discharge rate of the one-lane segment, we have $F'J' = \frac{\frac{k_j}{2}}{(\frac{1}{v_u}+\frac{1}{w})} = \frac{k_j \cdot v_u \cdot w}{2(v_u+w)}$. As the angle of $\angle G'OI' = arctan\, v_u$, OJ' can be calculated as $OJ' = \frac{F'J'}{v_u} = \frac{k_j \cdot w}{2(v_u+w)}$. As the angle of $\angle G'I'O = arctan\, w$, $J'L'$ can be calculated as $J'L' = \frac{F'J'}{w_m} = \frac{k_j \cdot v_u}{2(v_u+w)}$. As the angle of $\angle I'OI = arctan\, v_{lt}$, JJ' can be calculated as $JJ' = OJ' \cdot v_{lt} = \frac{k_j \cdot w \cdot v_{lt}}{2(v_u+w)}$. Then, the maximum discharge rate of the moving bottleneck in the moving coordinates with a value of FJ' can be calculated as

$$FJ' = F'J' - JJ' = \frac{k_j \cdot v_u \cdot w}{2(v_u + w)} - \frac{k_j \cdot w \cdot v_{lt}}{2(v_u + w)} = \frac{k_j \cdot w \cdot (v_u - v_{lt})}{2(v_u + w)} \quad (3.5)$$

However, the most important calculation is the maximum discharge rate of point H' in the stationary coordinates, i.e., the length of $H'M'$. In the moving coordinates, we have the same flow at points F and H, which means that $HM' = FJ' = \frac{k_j \cdot w \cdot (v_u - v_{lt})}{2(v_u+w)}$. As $G'K'$ is the maximum discharge rate of the two-lane segment, we have $G'K' = \mu_m = \frac{k_j}{(\frac{1}{v_u}+\frac{1}{w})} = \frac{k_j \cdot v_u \cdot w}{v_u+w}$, and as the angle of $\angle G'I'O = arctan\, w$, $K'I'$ can be calculated as $K'I' = \frac{G'K'}{w} = \frac{k_j \cdot v_u}{v_u+w}$.

Suppose the density at point H' is k, we have $w = \frac{H'M'}{M'I'} = \frac{HM'+kv_{\mathrm{lt}}}{k_j-k} = \frac{\frac{k_j \cdot w \cdot (v_{\mathrm{u}}-v_{\mathrm{lt}})}{2(v_{\mathrm{u}}+w)}+kv_{\mathrm{lt}}}{k_j-k}$ and, thus, the density at point H' can be calculated as $k = \frac{k_j \cdot w}{2}\left(\frac{1}{v_{\mathrm{u}}+w} + \frac{1}{v_{\mathrm{lt}}+w}\right)$. The effective discharge rate of point H' in the stationary coordinates, i.e., the length of $H'M'$ can be calculated via Equation (3.6).

$$\begin{aligned} \mu' = H'M' = HM' + kv_{\mathrm{lt}} &= \frac{k_j \cdot w \cdot (v_{\mathrm{u}} - v_{\mathrm{lt}})}{2(v_{\mathrm{u}} + w)} + \frac{k_j \cdot w \cdot v_{\mathrm{lt}}}{2}\left(\frac{1}{v_{\mathrm{u}} + w} + \frac{1}{v_{\mathrm{lt}} + w}\right) \\ &= \frac{k_j \cdot v_{\mathrm{u}} \cdot w}{v_{\mathrm{u}} + w} \cdot \frac{2v_{\mathrm{lt}} \cdot v_{\mathrm{u}} + w \cdot v_{\mathrm{u}} + w \cdot v_{\mathrm{lt}}}{2(v_{\mathrm{lt}} + w) \cdot v_{\mathrm{u}}} \\ &= \mu \cdot \frac{2v_{\mathrm{u}} \cdot v_{\mathrm{lt}} + v_{\mathrm{lt}} \cdot w + w \cdot v_{\mathrm{u}}}{2(v_{\mathrm{lt}} + w) \cdot v_{\mathrm{u}}} \end{aligned} \tag{3.6}$$

In this way, the effective discharge rate of the moving bottleneck in the stationary system in Figure 3.2 has now been derived. If we use a new variable θ and make $\theta = \frac{2v_{\mathrm{u}} \cdot v_{\mathrm{lt}} + v_{\mathrm{lt}} \cdot w + w \cdot v_{\mathrm{u}}}{2(v_{\mathrm{lt}}+w) \cdot v_{\mathrm{u}}}$, Equation (3.6) becomes $\mu' = \mu \cdot \theta$, in which θ is, essentially, the capacity discount factor due to the moving bottleneck caused by the ATMA. In other words, before the ATMA vehicles enter the road, the roadway capacity is μ, and as soon as the ATMA vehicles enter the roadway segment, it creates a moving bottleneck with an effective discharge rate of μ', given by Equation (3.6), until the ATMA vehicles depart the roadway segment.

3.3 LOS Derivation

As discussed earlier, learning from HCM, we choose total delay, as well as traffic density, as the performance measurements, to quantitatively evaluate the impact of the ATMA vehicles on traffic flow, and support the identification of ODD. The main input data is the

demand profile, i.e., AADT, and the K-factor (i.e., proportion of AADT occurring in the peak hour), as well as D-factor (i.e., the peak-hour volume proportion in the major direction). HCM recommends that the peak 15-min flow rate is used for most of the analytical procedures, so the Peak Hour Factor (PHF) is also considered as an input.

To be consistent with the notations in the earlier sections, we use $\lambda(\tau)$ as the traffic demand input, considering the 15-min flow rate. Based on AADT, the K-factor, the D-factor, the hourly traffic demand $\lambda(\tau)$ can be derived by directional design hourly volume (DDHV) and PHF via Equation (3.7).

$$\lambda(\tau) = \frac{DDHV}{PHF} = \frac{AADT \times K \times D}{PHF} \tag{3.7}$$

Next, by combining the discounted capacity from Equation (3.6) and demand profile from Equation (3.7), we derive the vehicle delay, as well as the traffic density, as follows.

First, the queue length during the ATMA maintenance can be calculated as $Q(t) = \int_0^t (\lambda(\tau) - \mu')d\tau$, i.e., the number of vehicles sitting in the queue is the difference between demand and discharge rates.

Next, according to Equation (2.2), the total delay caused by the AMTA vehicles during maintenance on a roadway segment can be calculated as $W = \int_0^{\frac{L}{v_{lt}}} Q(t)dt$, in which L is the length of the roadway segment. The total number of vehicles that enter a roadway segment is $N = \int_0^{\frac{L}{v_{lt}}} \lambda(\tau)d\tau$. Thus, the average delay of each passenger vehicle can be computed as Equation (3.8).

$$\bar{W} = \frac{W}{N} = \frac{\int_0^{\frac{L}{v_{\mathrm{lt}}}} Q(t)dt}{\int_0^{\frac{L}{v_{\mathrm{lt}}}} \lambda(\tau)d\tau} \tag{3.8}$$

Then, the average travel time on this four-lane highway segment can be calculated as Equation (3.9).

$$\bar{t} = \frac{L}{v_{\mathrm{u}}} + \bar{W} \tag{3.9}$$

Now that the average travel time is known, we can easily convert it back to the average speed of a vehicle travelling on the roadway segment and determine the density of the roadway segment. To do this, we first compute the average travel speed $\bar{v}$, as shown in Equation (3.10). Then, the density on this four-lane highway segment $\tilde{k}$ can be estimated as in Equation (3.11). Thus, the level of service on the highway segment can be determined by looking up to HCM [7], or using the density thresholds in Figure 2.2.

$$\bar{v} = \frac{L}{\bar{t}} \tag{3.10}$$

$$\tilde{k} = \frac{DDHV}{2\bar{v} \times PHF} = \frac{AADT \times K \times D}{2\bar{v} \times PHF} \tag{3.11}$$

Chapter 4 Numerical Analysis

4.1 Effective Discharge Rate Validation

To validate the effective discharge rate discount factor equation that is derived in Equation (3.6), the NGSIM dataset is used. This is because the validation of a roadway capacity model requires information on all vehicles on the roadway segment and, as such, the NGSIM dataset (which includes high-resolution trajectory of every single vehicle) becomes the ideal dataset to use. We focus on the dataset for Northbound I-80 in Emeryville, California (shown in Figure 4.1). The study target includes lane 5 and lane 6, with a length of approximately 1,090 ft.

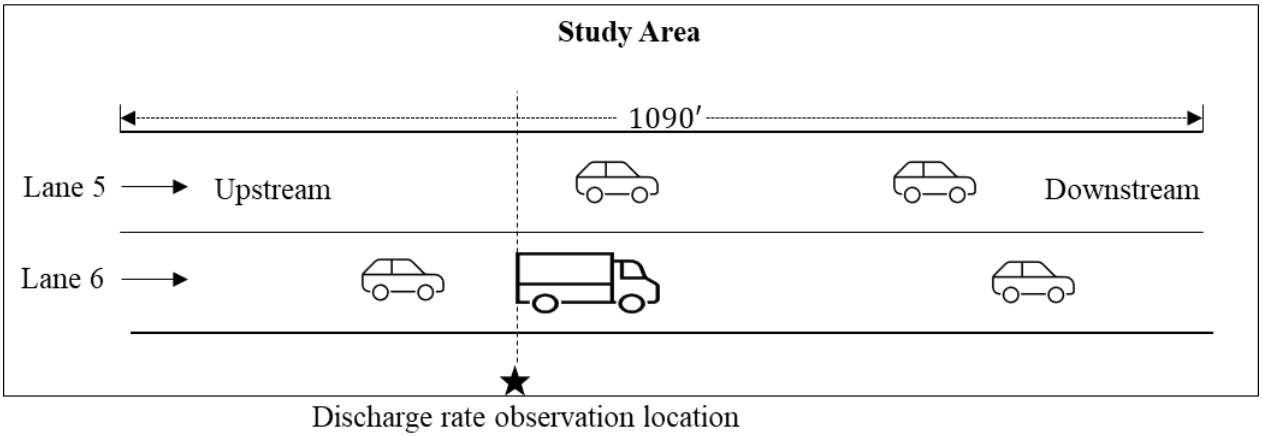

Figure 4.1 An illustration of the study area: Northbound I-80.

An open-source software, DTALite/NeXTA [22], is used to import NGSIM vehicle trajectories and to extract jam density, backward wave speed, and other needed characteristics. For the analyzed scenario, the vehicle trajectories in a time-space diagram for lane 5 and lane 6, between 04:00 p.m. and 04:15 p.m., and between 05:00 p.m. and 05:30 p.m. on April 13, 2005, are used. Figure 4.2 below illustrates the vehicle trajectories in a time space diagram for lanes 5 and 6. The areas highlighted by red rectangles A~E show the shockwave propagation in the

NGSIM dataset. The slopes of these shockwaves range from 10 mph to 14 mph and, as such, the average backward wave speed is set at 12 mph. The jam density is set as 180 veh/lane/mile, and a cruising speed of 30 mph is used. According to Equation (2.1), the maximum discharge rate of the traffic stream can be calculated as $\mu = \frac{2k_j \cdot v_u \cdot w}{v_u + w} = 3{,}076$ veh/hr.

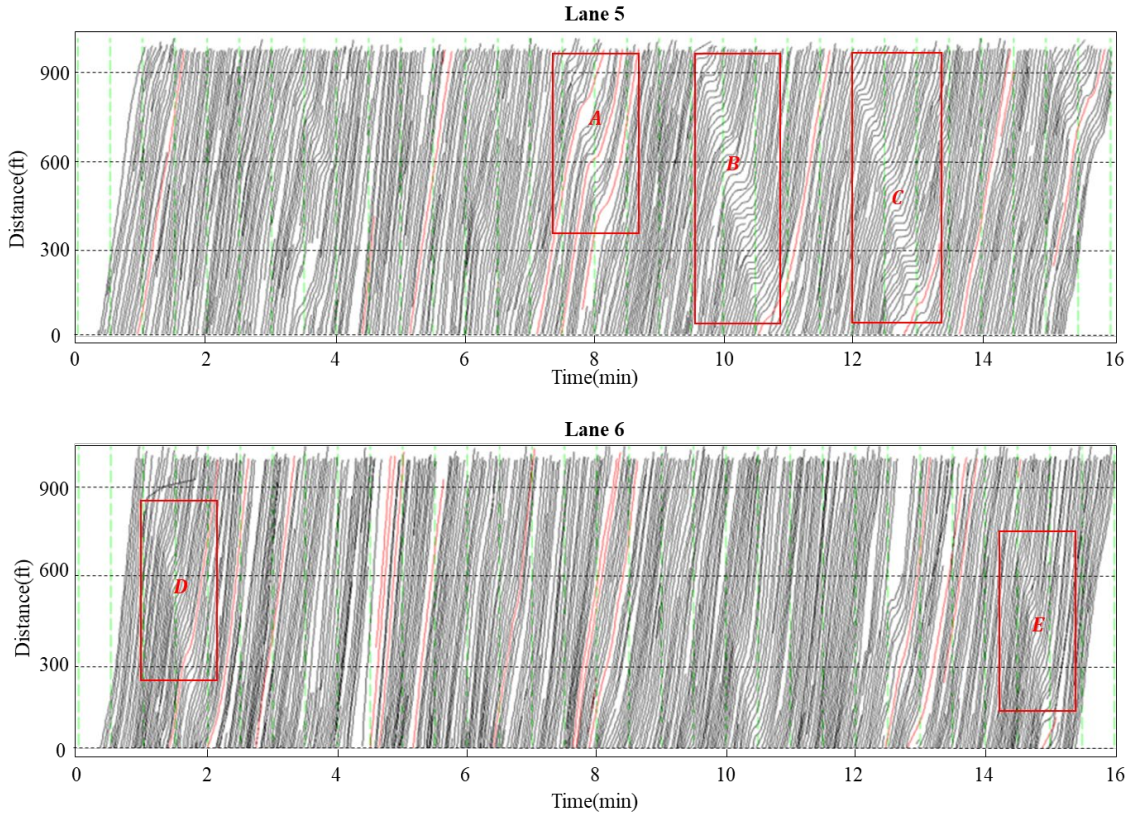

Figure 4.2 Vehicle trajectory for lanes 5 and 6, I-80, NGSIM.

To validate the effective discharge rate, we need to collect the ground truth discharge rate when affected by a moving bottleneck. To do so, we choose a fixed location (as shown by the star in Figure 4.1) as the location for observation. A total of six slow-moving trucks are observed on lane 5 and lane 6, between 04:00 p.m. and 04:15 p.m., and between 05:00 p.m. and 05:30 p.m.

In other words, we observed a total of six moving bottlenecks. The time-space diagrams of two representative moving bottlenecks, generated by two slower trucks with ID 2862 and 1522, are shown in Figure 4.3, in which red curves represent trucks, and black curves stand for other general vehicles. For the sake of simplicity, we only show the time-space diagram of two trucks below.

In Figure 4.3 (a), the slower truck (ID: 2862) is driving in lane 6 at a travel speed of 11 mph. Based on the time-space diagram of lane 6, we can tell the slope of the truck trajectory is lower than that of the other vehicles, indicating that the truck is moving slower than the surrounding traffic. It can also be found that the vehicle that follows this truck has a broken trajectory in lane 6, meaning that it chooses to switch to the left lane in order to bypass the slow-moving bottleneck. Based on the time-space diagram, the ground truth discharge rate is found to be approximately 2,740 veh/hr, for lanes 5 and 6 combined. In other words, $\mu_{GTD} = 2{,}740$ veh/hr. According to Equation (3.6), the discount factor of the effective discharge rate can be calculated as $\theta = 0.83$, and the effective discharge rate is $\mu' = 2{,}568$ veh/hr. Comparing μ' and μ_{GTD}, the absolute percentage error (APE) can be calculated as $APE_1 = \frac{|2{,}568-2{,}740|}{2{,}740} = 6.3\%$. On the other hand, if we ignore the impact of the moving bottleneck and directly use the maximum discharge rate μ, by comparing μ and μ_{GTD}, the APE would become $APE_2 = \frac{|3{,}076-2{,}740|}{2{,}740} = 12.3\%$. Comparison of APE_1 and APE_2 suggests that using the proposed effective discharge rate is more reasonable than directly using the maximum discharge rate, and the resulting APE drops from 12.3% to 6.3%.

Figure 4.3(b) presents the time space diagram of the moving bottleneck generated by another slower truck (ID: 1522) with a traveling speed of 5 mphr. The ground truth discharge rate can be observed and approximately equals $\mu_{GTD} = 1{,}982$ veh/hr. The effective discharge

rate can be calculated as $\mu' = 2{,}127$ veh/hr. Thus, the APE can be calculated as $APE_1 = \frac{|2{,}127-1{,}982|}{1{,}982} = 9.5\%$, when compared with the ground truth discharge rate. However, the APE will become $APE_2 = \frac{|3{,}076-1{,}982|}{1{,}982} = 55.2\%$ if the impact of the moving bottleneck is ignored. The resulting APE drops from 55.2% to 9.5%, a significant improvement.

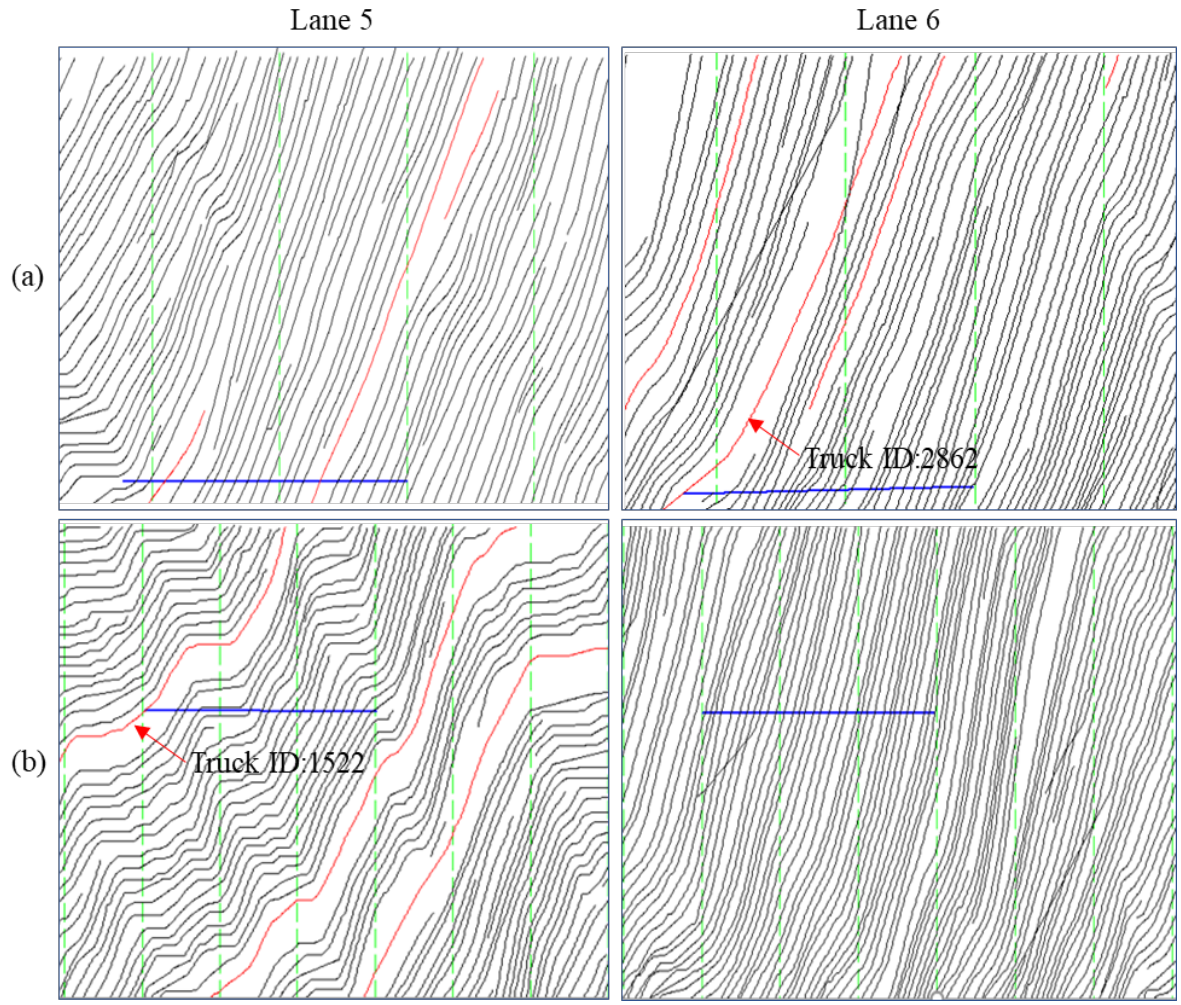

Figure 4.3 Vehicle trajectory of trucks (IDs:2862 and 1522), I-80, NGSIM.

Figure 4.4 shows the APE comparison of all six moving bottlenecks caused by those slow-moving trucks. It can be found that the maximum discharge rate μ (represented by the red

solid line) always overestimates the ground truth discharge rate μ_{ground} (the black line), with APE_2 (the red dashed line) ranging from 12.3% to 55.2%. On the other hand, the proposed model can calibrate the effective discharge rate μ' (the blue solid line) much closer to the ground truth discharge rate μ_{ground}, with APE_1 (the blue dashed line) ranging from 6.3% to 13.6%. These numbers demonstrate that the proposed model can generate satisfactory traffic capacity associated with moving bottlenecks in traffic flow.

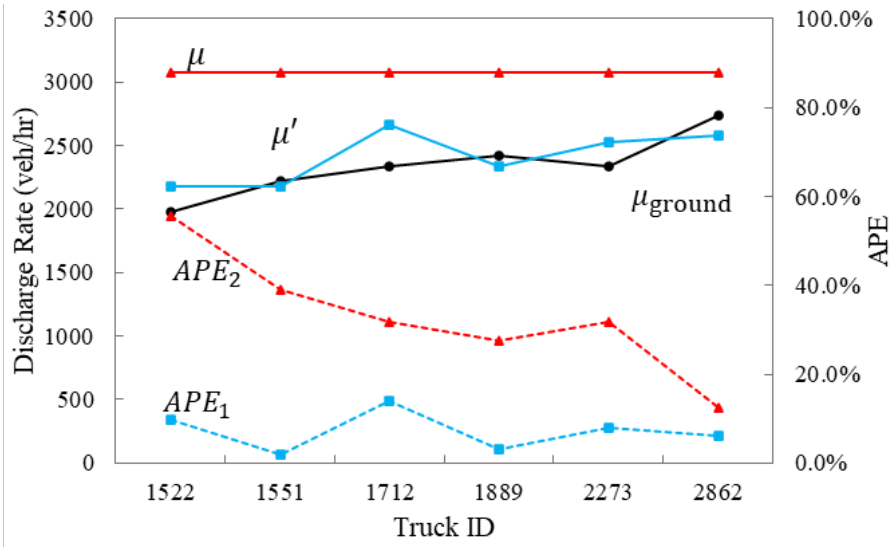

Figure 4.4 APE comparison of six slower trucks, I-80, NGSIM.

4.2 Typical Scenario ODD Analysis

In this section, an analysis of the impact of the ATMA on the traffic flow of a typical highway, including traffic delay and resulting density identifies the potential ODD of this technology. The analysis target is a four-lane highway segment, as shown in Figure 3.1. The characteristics of this analyzed highway segment are set as follows: $L = 1$ mile, $v_{\text{lt}} = 10$ mph, $v_{\text{u}} = 50$ mph, $w = 12$ mph, $k_{\text{j}} = 190$ veh/mile/lane. Traffic volumes on multilane

highways vary widely but often have demand in a range of 15,000 to 40,000 veh/day, while volumes as high as 100,000 veh/day have been observed in some cases [7]. Thus, we set the AADT as ranging from 15,000 veh/day to 60,000 veh/day. Recommended by HCM, the values of representative K, D factors and PHF are set as 0.09, 0.6, and 0.9 to represent urban and rural areas, respectively. The hourly traffic demand can be estimated by Equation (3.7).

Based on the setup of highway geometry and traffic flow characteristics, the relationship between traffic demand (i.e., AADT), vehicle delay, and traffic density are shown in Figure 4.5. The average vehicle delay, denoted by the black dotted line, remains zero before the traffic demand AADT reaches 45,000 vehicles per day. After that, the average delay increases sharply from 0 to 36 seconds per vehicle. The red line stands for the traffic density, which increases at a relatively slow speed from 9 veh/mile/lane to 24 veh/mile/lane, when the AADT is no more than 40,000 veh/day. However, after that, the density increases at a much faster pace.

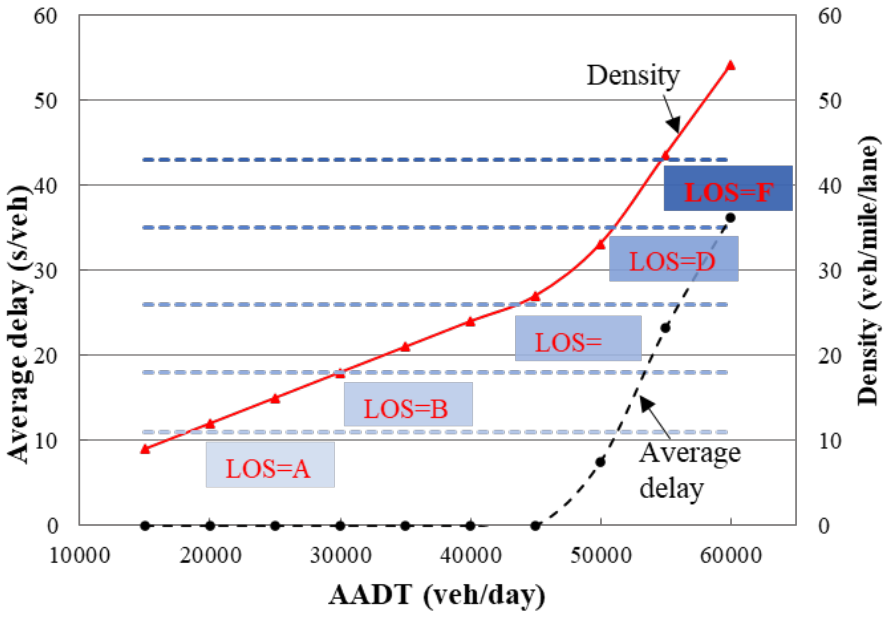

Figure 4.5 Relationship between AADT, average vehicle delay and traffic density.

We also identify level of service based on density. Learning from Figure 2.2, the density thresholds that differentiate LOS are 11, 18, 26, 35, and 45, respectively, and we use them to define the LOS category in Figure 4.5 as well. Figure 2.2 also tells us that, when LOS is from A to C, the traffic speed does not fluctuate much, and we know that a low speed fluctuation is important for work zone safety. As such, we use LOS=C as a desirable design objective for ATMA's operation design domain, which corresponds to between 40,000 and 45,000 AADT in Figure 4.5. As can be seen from the figure, when AADT is below 40,000, the delay is zero, where density is relatively low at a value of less than 26 vehicle/lane/mile, and the traffic flow remains at free flow speed. In other words, at this traffic level, drivers do not experience significant traffic disruption and they do not even need to significantly change their speed. As such, for this typical scenario, the AADT of 40,000 is identified as a good threshold for defining ATMA's ODD.

4.3 Sensitivity Analysis

In this section, sensitivity analysis is performed to show how changing the K factor, D factor, and operating speed of ATMA vehicles can influence the total delay and density during maintenance. According to HCM [7], the range of the D factor is set to be 0.5~0.65, with the K factor as 0.08 to 0.11. The operating speeds of ATMA vehicles range from 5~15 mph. Thus, the ODD of the ATMA can be analyzed in accordance with the results of sensitivity analysis.

When D-factor changes

Figure 4.6 presents the proposed relationship between traffic demand (i.e., AATD), average delay (illustrated in Figure 4.6-a), and density (illustrated in Figure 4.6-b), when factor D changes from 0.5 to 0.65.

Figure 4.6-a shows that, the average delay remains zero at first, but increases sharply once the AADT is beyond a threshold. As we can see, the average delay increases from 0 to 8 sec/veh when D is 0.5, whereas the average delay increases from 0 to 47 sec/veh as D changes to 0.65. The AADT threshold for a delay to start increasing, is about 55,000, when D is 0.5, but as the D value increases, this AADT threshold reduces to 50,000, 45,000, and 40,000, respectively.

Similarly, Figure 4.6-b shows that the density increases at a much slower speed, until AADT reaches a threshold, after which the density increases much faster. As the D value increases, the traffic flow becomes denser. When D is set to be 0.5, the density increases slightly from 8 veh/mile/lane to 25 veh/mile/lane, and the LOS decreases from A to C before the AADT reaches 50,000 veh/day. Once the AADT is greater than 50,000 veh/day, the density increases significantly from 25 veh/mile/lane to 33 veh/mile/lane, and the LOS becomes worse from C to D. As D changes to 0.65, the density increases slightly from 10 veh/mile/lane to 26 veh/mile/lane, and the LOS decreases from A to C before the AADT reaches 40,000 veh/day. Once the AADT is greater than 40,000 veh/day, the density increases significantly from 26 veh/mile/lane to 65 veh/mile/lane, and the LOS becomes worse from C to F. Combined from the above analysis, when the D factor increases from 0.5, to 0.55, 0.6, and then to 0.65, the corresonding AADT thresholds to define ATMA ODD are 50,000, 45,000, 45,000, and 40,000, respectively.

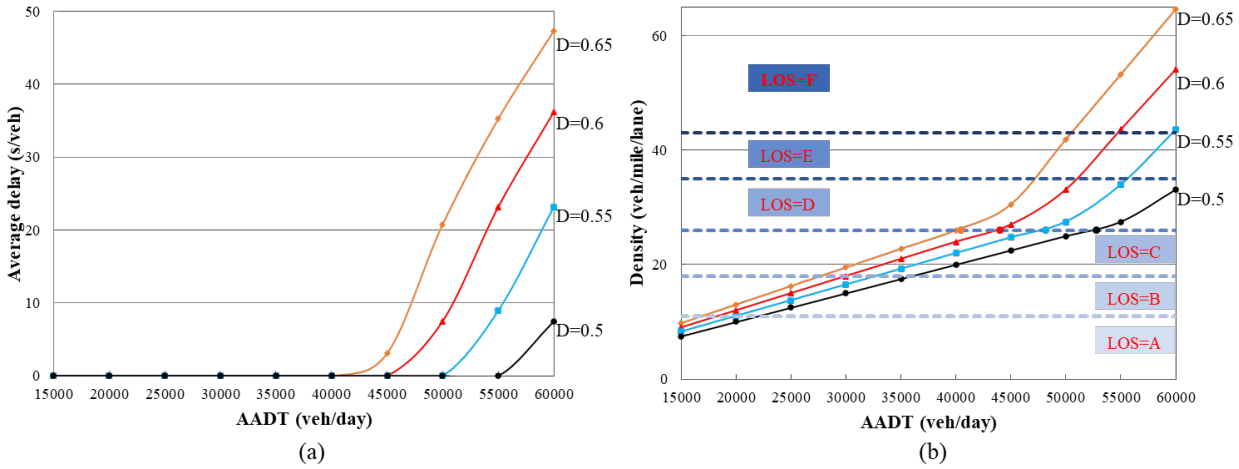

Figure 4.6 Proposed relationship between AADT and (a) average delay and (b) LOS when D changes.

4.3.1 When K-factor changes

In this section, we examine what will happen if the K factor changes. Figure 4.7 presents the relationship between traffic demand (i.e., AATD), average delay (illustrated in Figure 4.7-a) and density (illustrated in Figure 4.7-b), when K changes from 0.08 to 0.11. The observed pattern is similar when D changes.

Figure 4.7 shows that the average delay and density increases sharply once the AADT reaches certain thresholds. When K is set to be 0.08, the average delay remains as zero, until the AADT increases to higher than 50,000. After that, the delay increases from 0 to 18 sec/veh. As for the density, it only increases slightly from 8 veh/mile/lane to 24 veh/mile/lane (corresponding to LOS A~C), before the AADT reaches 50,000 veh/day. Once the AADT is higher than that, the density increases significantly from 24 veh/mile/lane to 40 veh/mile/lane, and the LOS becomes worse to E.

Similar trends can also be found for the other curves, corresponding to different K values. In general, when the K value increases, the AADT threshold reduces, and the delay and LOS

increases much faster. Combined with these curves, when the K factor increases from 0.08, to 0.09, 0.1 and, then, to 0.11, the corresonding AADT thresholds to define ATMA ODD are 50,000, 45,000, 40,000, and 35,000, respectively.

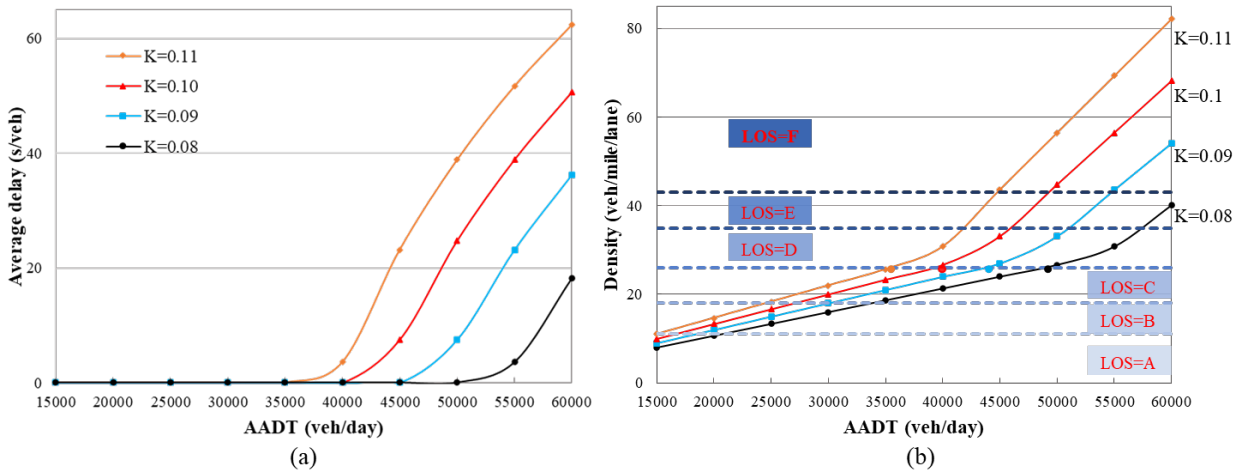

Figure 4.7 Proposed relationship between the AADT and (a) average delay and (b) LOS when K changes.

4.3.2 When operating speeds of the ATMA vehicles change

In this section, we examine what will happen if an ATMA's operating speed changes. Figure 4.8 presents the relationship between traffic demand (i.e., AATD), average delay (illustrated in Figure 4.8-a) and density (illustrated in Figure 4.8-b), when the ATMA's operating speed changes from 5 to 15mph. In this analysis, K is fixed at 0.09 and D is fixed at 0.6. The observed pattern is similar when K and D change.

Figure 4.8-a shows the average delay remains zero if the AADT is less than certain thresholds, which means the effective discharge rate satisfies the traffic demand. The average delay increases slightly from 7 sec/veh to 17 sec/veh when the ATMA operating speed is set to 15 mph. However, when the operating speed of ATMA vehicles is 5 mph, the average delay

increases sharply from 0 sec/veh to 109 sec/veh. This is because a slower ATMA operating speed corresponds to a slower moving bottleneck that discounts traffic capacity even more significantly. On the other hand, Figure 4.8-b shows a similar trend for density, that only increases slightly from 9 veh/mile/lane to 26 veh/mile/lane (corresponding to LOS A~C), before the AADT reaches 45,000 veh/day at an operating speed of 15 mph. If the AADT increases further to exceed this threshold, the resulting density will increase at a much faster pace.

Similar trends can also be found for the other curves that correspond to different ATMA operating speeds. In general, when an operating speed reduces, the AADT threshold reduces, and the delay and LOS increase much faster. Combined with these curves, when operating speeds reduce from 15 mph to 10 mph, and then to 5 mph, the corresonding AADT thresholds to define ATMA ODD are 45,000, 45,000, and 40,000, respectively.

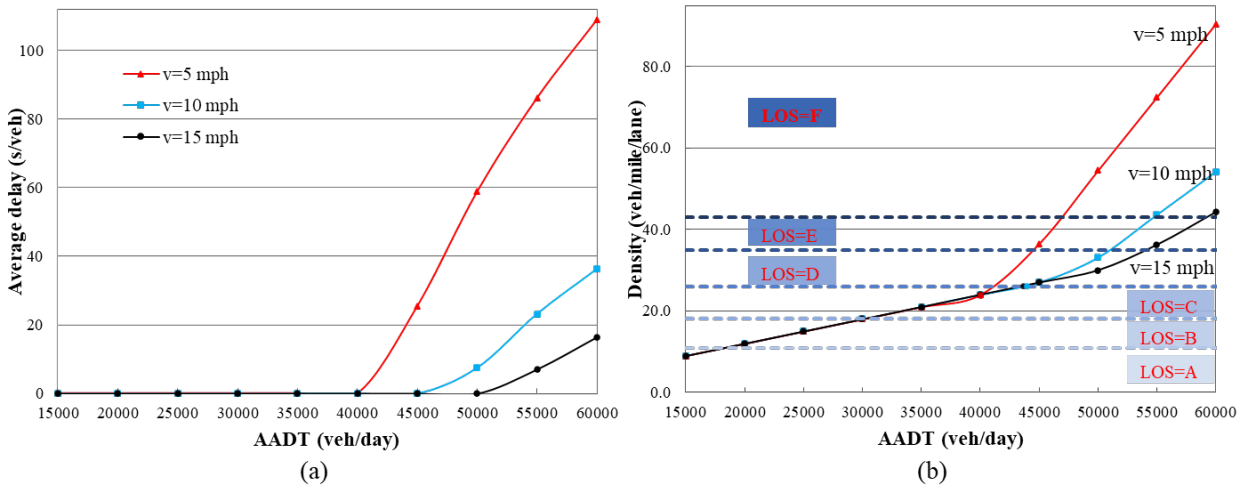

Figure 4.8 Proposed relationship between the AADT and (a) average delay and (b) LOS when the operating speed of an ATMA changes.

Chapter 5 Conclusions

This project aims to identify the operational design domain for an AMTA vehicle system, for transportation infrastructure maintenance on multilane highways, and at work zones. First, the effective discharge rate of a roadway segment is analytically derived, considering the moving bottleneck caused by slow-moving ATMA vehicles. The formulation is based on the fundamental diagram with moving coordinates. The derived effective discharge rates are represented with simple mathematical expressions in a closed-form, and correctly account for the effects of demand inputs and real time traffic status, as well as traffic flow characteristics. Next, microscopic traffic flow models are employed, so that once the discounted capacity is obtained, it can be combined with the highway traffic arrival rates to calculate vehicle delay and traffic flow density. These are chosen as the key indicators of a multilane highway's level of service. In this way, the linkage between demand (e.g., AADT) and LOS are analytically established and numeric analysis is performed based on these relationships to quantitively determine the ODD of the ATMA.

Validation with NGSIM data shows that our model correctly captures the effective discharge rate discount affected by moving bottlenecks, that results in an estimation error ranging from 6.3% to 13.6%, indicating a satisfactory result. Modeling result analysis, under a typical scenario (K=0.09, D=0.6 and PHF=0.9), shows that, if we use LOS=C as a desirable design objective for ATMA's operation design domain, the corresponding AADT threshold is 40,000. This means that, when AADT is below 40,000, the traffic flow remains at free flow speed, the delay is almost zero, and the density is relatively low with a value of less than 26 vehicle/lane/mile. In other words, at this traffic level, drivers do not experience significant traffic disruption and they do not even need to significantly change their speed. As such, for this typical

scenario, the AADT 40,000 is identified as a good threshold for defining an ATMA's ODD. Sensitivity analysis is also performed, and shows that when K factor, D factor, or ATMA operating speed changes, the AADT threshold will change correspondingly.

References

1. ASCE. *Report Card for America's Infrastructure* 2020; Available from: https://infrastructurereportcard.org/cat-item/roads/.

2. MoDOT, *Leader-Follower Truck Mounted Attenuator System Request for Proposal*. 2018, Missouri Department of Transportation: Jefferson City, Missouri.

3. *Skip Descant, Colorado DOT Launches Autonomous Vehicles to Improve Worker Safety*. 2017; Available from: https://www.govtech.com/fs/data/Colorado-DOT-Launches.

4. Tang, Q., et al., *Evaluation Methodology of Leader-Follower Autonomous Vehicle System for Work Zone Maintenance.* Transportation Research Record, 2021. 0(0): p. 0361198120985233.

5. Inc., R.T.E. *Autonomous TMA Truck to Provide Insights to TDOT for Improving Work Zone Safety*. 2019; Available from: https://www.prnewswire.com/news-releases/autonomous-tma-truck-to-provide-insights-to-tdot-for-improving-work-zone-safety-300951862.html.

6. CDOT. *Autonomous Maintenance Technology (AMT) Pool Fund*. 2018; Available from: http://www.csits.colostate.edu/autonomous-maintenance-technology.html.

7. *Highway Capacity Manual*. 2010: Transportation Reseach Board.

8. Leclercq, L., J.A. Laval, and N. Chiabaut, *Capacity Drops at Merges: an endogenous model.* Procedia - Social and Behavioral Sciences, 2011. 17: p. 12-26.

9. Leclercq, L., et al., *Capacity drops at merges: New analytical investigations.* Transportation Research Part C: Emerging Technologies, 2016. 62: p. 171-181.

10. Leclercq, L., et al., *Capacity Drops at Merges: Analytical Expressions for Multilane Freeways.* Transportation Research Record, 2016. 2560(1): p. 1-9.

11. Yuan, K., V.L. Knoop, and S.P. Hoogendoorn, *A Microscopic Investigation Into the Capacity Drop: Impacts of Longitudinal Behavior on the Queue Discharge Rate.* Transportation Science, 2017. 51(3): p. 852-862.

12. Laval, J.A. and C.F. Daganzo, *Lane-changing in traffic streams.* Transportation Research Part B: Methodological, 2006. 40(3): p. 251-264.

13. Chen, D. and S. Ahn, *Capacity-drop at extended bottlenecks: Merge, diverge, and weave.* Transportation Research Part B: Methodological, 2018. 108: p. 1-20.

14. Menendez, M. and C.F. Daganzo, *Effects of HOV lanes on freeway bottlenecks.* Transportation Research Part B: Methodological, 2007. 41(8): p. 809-822.

15. Laval, J.A. and L. Leclercq, *Microscopic modeling of the relaxation phenomenon using a macroscopic lane-changing model.* Transportation Research Part B: Methodological, 2008. 42(6): p. 511-522.

16. Monamy, T., H. Haj-Salem, and J.-P. Lebacque, *A Macroscopic Node Model Related to Capacity Drop.* Procedia - Social and Behavioral Sciences, 2012. 54: p. 1388-1396.

17. Parzani, C. and C. Buisson, *Second-Order Model and Capacity Drop at Merge.* Transportation Research Record, 2012. 2315(1): p. 25-34.

18. Jin, W.-L., Q.-J. Gan, and J.-P. Lebacque, *A kinematic wave theory of capacity drop.* Transportation Research Part B: Methodological, 2015. 81: p. 316-329.

19. Newell, G.F., *A simplified car-following theory: a lower order model.* Transportation Research Part B: Methodological, 2002. 36(3): p. 195-205.

20. Newell, G.F., *Applications of Queueing Theory*. Ettore Majorana International Science Series. 1982: Springer Netherlands.

21. Newell, G.F., *A moving bottleneck.* Transportation Research Part B: Methodological, 1998. 32(8): p. 531-537.

22. Zhou, X. and J. Taylor, *DTALite: A queue-based mesoscopic traffic simulator for fast model evaluation and calibration.* Cogent Engineering, 2014. 1(1): p. 961345.